Biochemistry

pubs.acs.org/biochemistry

Communication

Discovery and Characterization of a Novel Allosteric Small-Molecule Inhibitor of NADP$^+$-Dependent Malic Enzyme 1

Tomohiro Yoshida, Tetsuhiro Kawabe, Lewis C. Cantley, and Costas A. Lyssiotis*

Cite This: *Biochemistry* 2022, 61, 1548−1553

Read Online

ACCESS | Metrics & More | Article Recommendations | Supporting Information

ABSTRACT: NADP$^+$-dependent malic enzyme 1 (ME1) decarboxylates malate to form pyruvate and NADPH in the cytoplasm, where it mediates diverse biological functions related to the generation of lipids and other cellular building blocks. As such, ME1 has been implicated in the progression of cancers and has received attention as a promising drug target. Here we report the identification of a novel small-molecule inhibitor of ME1, designated AS1134900. AS1134900 is highly selective for ME1 compared with ME2 and uncompetitively inhibits ME1 activity in the presence of its substrates NADP$^+$ and malate. In addition, X-ray crystal structure analysis of the enzyme−inhibitor complex revealed that AS1134900 binds outside the ME1 active site in a novel allosteric site. Structural comparison of the ME1 quaternary complex with AS1134900, NADPH, and Mn^{2+}, alongside known crystal structures of malic enzymes, indicated the determined crystal ME1−inhibitor complex is in the open form conformation. These results provide insights and a starting point for further discovery of drugs that inhibit ME1 activity in cancer cells.

Malic enzymes make up a family of enzymes that catalyze the oxidative conversion of malate to pyruvate and CO_2. The production of pyruvate serves as a component of the glycolytic and citric acid pathways.[1] Moreover, these enzymes mediate lipid and fatty acid biosynthesis through the generation of NADPH.[1] In mammals, malic enzymes have three isoforms: the cytosolic NADP$^+$-dependent malic enzyme (ME1), the mitochondrial NAD(P)$^+$-dependent malic enzyme (ME2), and mitochondrial NADP$^+$-dependent malic enzyme (ME3). Relative to mitochondrial ME2 and ME3, ME1 is located in the cytosol.

Multiple reports indicate that upregulated expression of ME1 in certain human cancers predicts poor prognosis.[2] In addition, knockdown of ME1 mRNA levels or inhibition of ME1 activity in tumor cell lines and mouse models inhibits tumor growth by accelerating oxidative stress, apoptosis, or senescence.[2,3] Therefore, the development of small-molecule inhibitors targeting ME1 may serve as a novel approach for treating cancer.

Although several small molecules derived from natural products have been reported as ME2 inhibitors,[4−6] the only such molecules known to inhibit ME1 activity are those based on the piperazine-1-pyrrolidine-2,5-dione scaffold, identified from a fragment-based screening.[6,7] To identify a novel scaffold of ME1 inhibitors, we performed a high-throughput screening of ME1 in a protein-based assay.

A diaphorase/resazurin-coupled assay was applied to measure ME1 enzymatic activity with a miniaturized well format[8] (Figure 1A). Diaphorase requires NADPH to convert the resazurin to the fluorescent molecule resorufin. Further, resorufin fluoresces at 585 nm, which distinguishes it from other dehydrogenase assays. Compared with dehydrogenase assays that detect the fluorescence of NADPH (excitation at 340 ± 30 nm, emission at 460 ± 50 nm), this "red-shifted" assay reduces the level of interference of blue fluorescence that

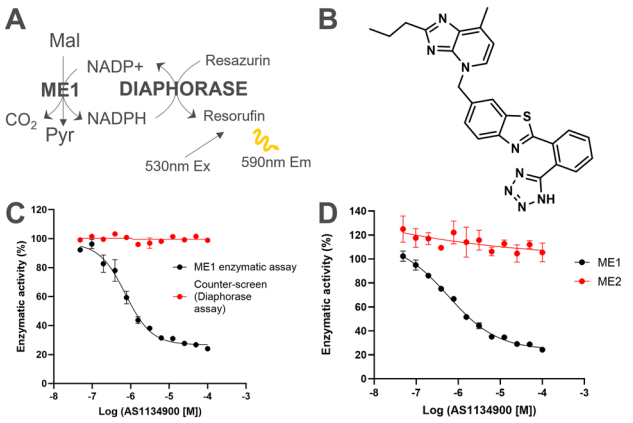

Figure 1. Structure and enzymatic inhibition profiles of AS1134900. (A) Diaphorase/resazurin-coupled ME1 assay for high-throughput screening. Mal, malate; Pyr, pyruvate. (B) Structure of 6-[(7-methyl-2-propylimidazo[4,5-*b*]pyridin-4-yl)methyl]-2-[2-(1*H*-tetrazol-5-yl)-phenyl]-1,3-benzothiazole (AS1134900). (C) Inhibition of ME1 activity by AS1134900 (black circles) and a counterscreen including only NADPH and diaphorase/resazurin in the reaction mixture (red circles). (D) Inhibition of ME1 and ME2 activities by AS1134900 (black circles, ME1; red circles, ME2).

is prominent in large chemical libraries.[8] Primary screening was conducted at 10 μM using a proprietary chemical library

Received: March 3, 2022
Revised: July 3, 2022
Published: July 12, 2022

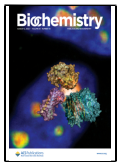

https://doi.org/10.1021/acs.biochem.2c00123
Biochemistry 2022, 61, 1548−1553

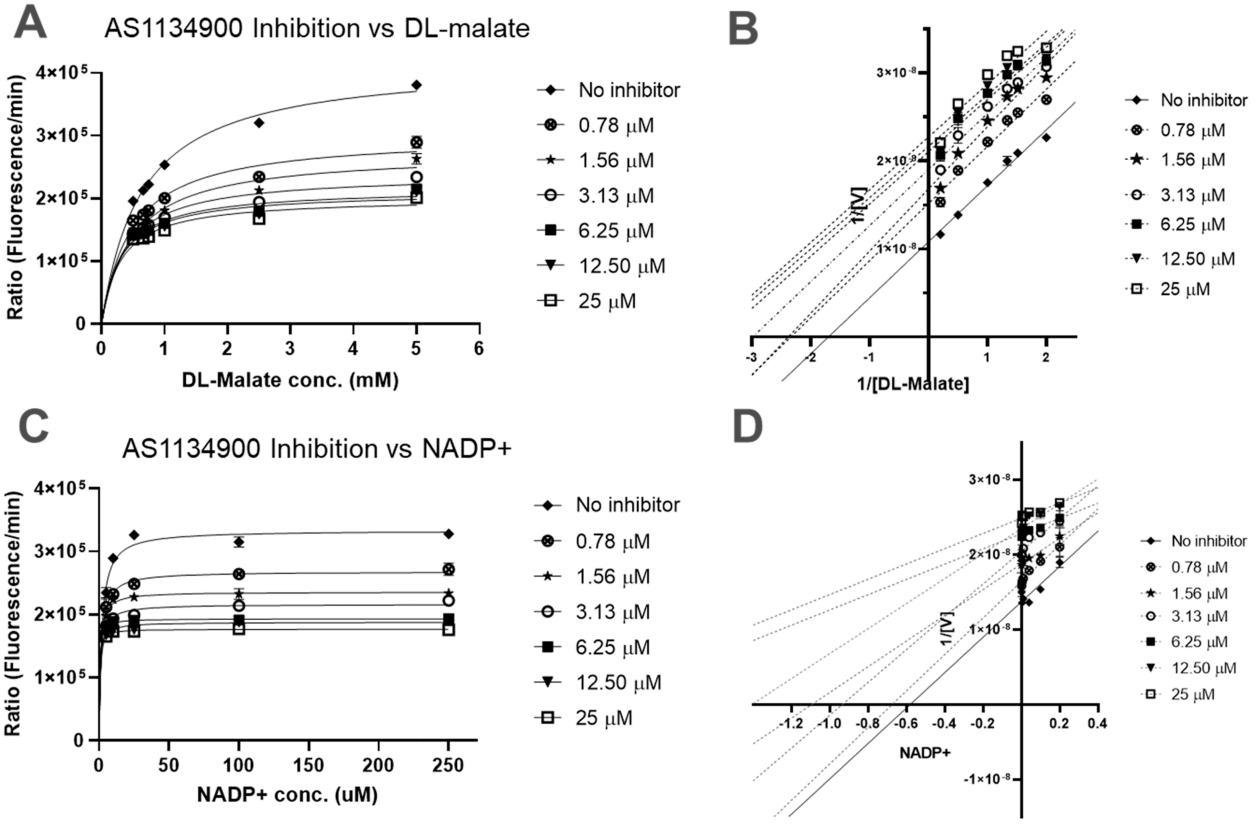

Figure 2. Mechanism of inhibition of ME1 by AS1134900. (A) Michaelis−Menten plot of ME1 activity in the presence of AS1134900 vs DL-malate. (B) Lineweaver−Burke plot of AS1134900 vs DL-malate. (C) Michaelis−Menten plot of AS1134900 vs $NADP^+$. (D) Lineweaver−Burke plot of AS1134900 vs $NADP^+$.

(Astellas Pharma). The mean signal to blank (S/B) of the screening campaign was 5.6 ± 0.61, and the Z' factor was 0.88 ± 0.033. The signal cutoff was set at 25% ME1 inhibition at a threshold equal to the average value + three standard deviations (SD). Primary hits were further evaluated to confirm a dose-dependent effect at a top concentration of 30 μM, and a counterscreen was performed to assess the effects on the diaphorase/resazurin assay. The following criteria were applied to identify hit compounds: IC_{50} of <30 μM, efficacy of >50%, and no observed dose response in the counterscreen.

From these collective efforts, we identified a potent small molecule, 6-[(7-methyl-2-propylimidazo[4,5-*b*]pyridin-4-yl)-methyl]-2-[2-(1*H*-tetrazol-5-yl)phenyl]-1,3-benzothiazole (designated AS1134900) (Figure 1B), with an IC_{50} of 0.73 μM in the ME1/resazurin assay (Figure 1C). AS1134900 did not inhibit the diaphorase/resazurin enzymatic reaction (Figure 1C). We next developed a mitochondrial NAD^+-dependent malic enzyme (ME2) assay to evaluate the selectivity of AS1134900 for ME isoforms. The positive control ATP inhibited ME2 activity (IC_{50} = 0.1 mM), which is consistent with the results of other studies (Figure S1).[5,9] In contrast, AS1134900 did not detectably inhibit ME2 (Figure 1D).

To elucidate the mechanism of inhibition of ME1 activity by AS1134900, enzyme kinetics were examined using various concentrations of malate or $NADP^+$. The K_m and V_{max} values of ME1 decreased as a function of AS1134900 concentration (Figure 2A,C). Moreover, the slopes of the Lineweaver−Burke plots were equal (Figure 2B,D). These results indicate that AS1134900 uncompetitively inhibited ME1 in the presence of $NADP^+$ and malate. The substrates are required for the binding of AS1134900 to ME1, where AS1134900 forms an abortive enzyme−NADPH−malate ternary complex.

We then conducted crystallographic analysis to identify the AS1134900-binding site of human ME1. Although the crystal structure of apo-ME1 has been published,[10] the crystal structure of ligand-bound ME1 is unknown. We therefore analyzed the ternary complex formed between NADPH and Mn^{2+} and determined the crystal structure [Figure S2, Figure 3A, Protein Data Bank (PDB) entry 7X12]. Consistent with published data,[10] this crystal structure of NADPH-bound ME1 formed an asymmetric tetramer unit with a root-mean-square deviation (RMSD) of 0.48 Å (Figure S2). In addition, superposition of NADPH-bound ME1 with the apo form of ME1 showed that the overall fold of these two structures is similar (RMSD of 0.73 Å) (Figure 3A).

We next determined the crystal structure of ME1 in the presence of AS1134900, NADPH, and Mn^{2+}. Under these conditions, ME1 formed a quaternary complex (PDB entry 7X11). Surprisingly, AS1134900 bound ME1 outside of the NADPH-binding site, between the α-helices of domains B (residues 131−277 and 464−535) and C (residues 278−463) (Figure 3B). In this complex, the benzothiazole moiety of AS1134900 was located below the benzene ring of Phe263, and the imidazo[4,5-*b*]pyridine moiety of AS1134900 was located above the imidazole ring of His321. These positions indicate $\pi-\pi$ stacking between the two individual aromatic rings (Figure 3C). Moreover, the carboxylate moiety of Asp485 lies in close proximity to the imidazo[4,5-*b*]pyridine moiety of AS1134900 (Figure 3C). We considered therefore that AS1134900 likely forms a hydrogen bond with the

https://doi.org/10.1021/acs.biochem.2c00123
Biochemistry 2022, 61, 1548−1553

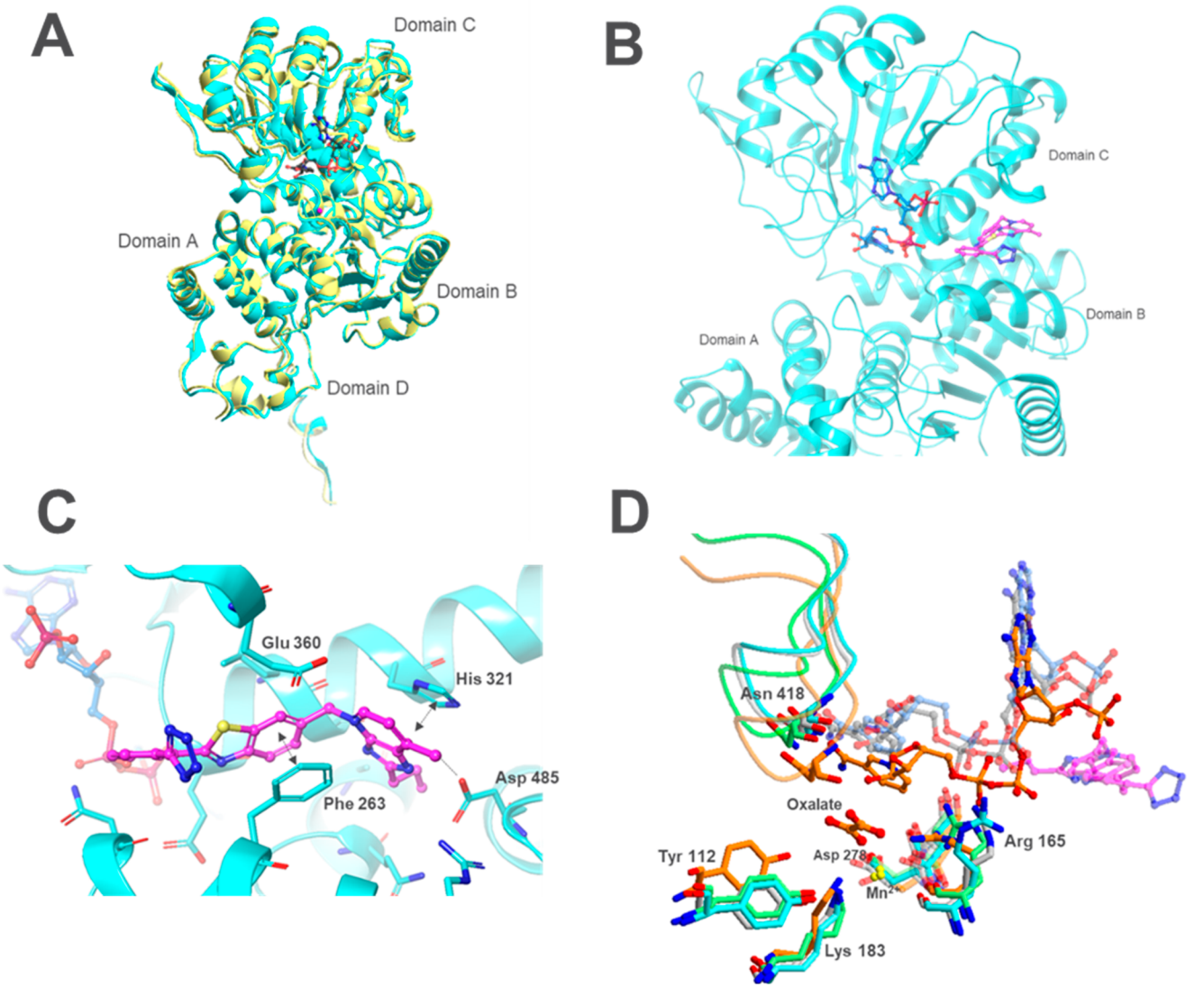

Figure 3. Crystal structure analysis of the AS1134900−ME1 complex. (A) Structural comparison of a monomer of apo-ME1 (yellow, PDB entry 3WJA) and an NADPH-bound form (cyan, PDB entry 7X12). NADPH in 7X12 is shown as a dark gray ball-and-stick model, and the Mn^{2+} ion is shown as a purple sphere. (B) ME1−AS1134900-binding site (cyan, PDB entry 7X11). The blue and purple ball-and-stick models indicate NADPH and AS1134900 molecules, respectively. (C) Three-dimensional depiction of the binding of AS1134900 to ME1 (cyan, PDB entry 7X11). The purple ball-and-stick model indicates AS1134900. (D) Structural comparison of the malic enzyme active site of the NADPH−AS1134900−human ME1 complex (cyan, PDB entry 7X11), NADPH-bound human ME1 (gray, PDB entry 7X12), apo-ME1 (green, PDB entry 3WJA), and the NADP−pigeon ME complex with $NADP^+$ and oxalate (orange, PDB entry 1GQ2). NADPH molecules in 7X11 and 7X12 are colored blue and gray, respectively. AS1134900 in 7X11 is colored purple. $NADP^+$ and oxalate in 1GQ2 are colored orange. Mn^{2+} ions are shown as yellow spheres.

nitrogen atom of imidazo[4,5-*b*]pyridine and carboxylate moieties of Asp485. When we overlaid the NADPH-bound ME1 (PDB entry 7X12) and NAPDH−AS1134900−ME1 complex (PDB entry 7X11), the slight movement of Val 260, Phe 263, His 321, Glu 360, and Asp 485 was observed, which we consider to be key residues for AS1134900 binding (Figure S3A). On the contrary, there is less influence of AS1134900 binding on the overall structure of NADPH-bound ME1, and superposition of these structures results in a high degree of similarity with an RMSD of 0.53 Å (Figure S3B).

Multiple crystal structures of malic enzymes in various complexed forms have been reported to date, and the enzymes likely are in equilibrium between open and closed forms with a conserved structural mechanism among different isoforms and species.[11−15] From these studies, a predominant model is one in which substrate binding in the active site at the interface of domains B and C shifts the open form to the closed form, which represents an active site closure. On the basis of substrate binding and closure of the active site, the side chains of Tyr 112 and Lys 183, as a presumable general acid−base pair in the oxidative decarboxylation of malate, conformationally change and catalyze the reaction.[14,15]

We therefore analyzed the conformational status of the active site for the NADPH−Mn^{2+}−ME1 and NADPH−AS1134900−Mn^{2+}−ME1 complexes by comparing them with known malic enzyme crystal structures. While crystal structures for ligand-bound ME1 are not available, the closed form of the c-NADP−pigeon ME crystal structure in a quaternary complex with $NADP^+$, Mn^{2+}, and oxalate (as a transition-state analogue of a substrate) has been reported[11] (PDB entry 1GQ2). Superposition of the active site of (i) the NADPH−AS1134900−human ME1 complex, (ii) NADPH-bound

https://doi.org/10.1021/acs.biochem.2c00123
Biochemistry 2022, 61, 1548−1553

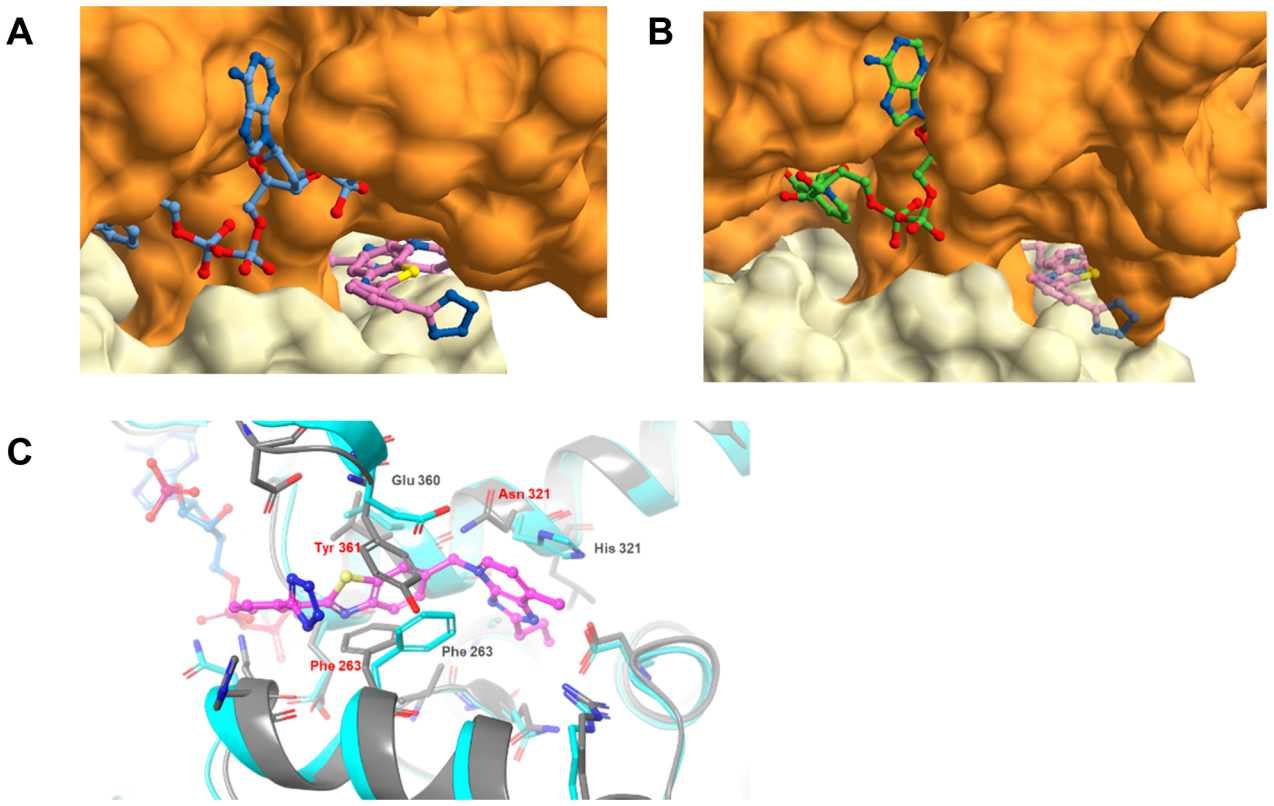

Figure 4. Crystal structure analysis of the AS1134900-binding site in ME1 and ME2. (A) Molecular surface depiction of NADPH- and AS1134900-binding sites of ME1 in PDB entry 7X11. Domain B is colored yellow, and domain C is colored orange. The blue and purple ball-and-stick models represent NADPH and AS1134900, respectively. (B) Molecular surface depiction of the NAD-binding site of ME2 in the open form (PDB entry 1QR6). Domain B is colored yellow, and domain C is colored orange. NAD in 1QR6 is shown as the green ball-and-stick model. (C) Three-dimensional depiction of the AS1134900-binding site of the NADPH−AS1134900−human ME1 complex (cyan, PDB entry 7X11) and superposition of the site of ME2 in the open form (gray, PDB entry 1QR6). The ball-and-stick model of the AS1134900 molecule (purple) in 7X11 is superposed on 1QR6.

human ME1, (iii) the NADP−pigeon ME complex bound to oxalate, and (iv) human apo-ME1 revealed large conformational differences among the side chains of Tyr 112 and Lys 183, which function as catalytic residues, and Arg 165 and Asn 418, which serve as key residues for substrate binding[15] (Figure 3D). The side chains of Tyr 112, Arg 165, Lys 183, and Asn 418 of the NADP−pigeon ME complex are close to oxalate to form ionic interactions with the substrate. This conformation shields the active site and represents a closed form. In contrast, the corresponding amino acids of the NADPH−AS1134900−human ME1 complex, NADPH-bound human ME1, and human apo-ME1 are located away from the substrate-binding site. Moreover, $NADP^+$ in the NADP−pigeon ME complex also comes closer to oxalate than the position of NADPH in the human ME1 crystal structures reported here.

Similarly, we then conducted a structural comparison of the active site of the NADPH−AS1134900−ME1 complex and both open[13] (PDB entry 1QR6) and closed forms[14] (PDB entry 1PJ3) of ME2 (Figure S4). The result was similar to that depicted in Figure 3D. The positions of the side chains of Tyr 112, Arg 165, Lys 183, and Asn 418 of the closed form of ME2 are closer to malate than those in the NADPH−AS1134900−ME1 complex and the open form of ME2. These results demonstrate the crystal structures of NADPH-bound ME1 and the NADPH−AS1134900−ME1 complex are both in the open form. Given that AS1134900 is an uncompetitive inhibitor (Figure 2) and thus binds only the ME1−substrate complex, we presume that the inhibitory activity of AS1134900 may be explained by the retention of the open form of the ME1−NADPH−malate intermediate complex through the binding of AS1134900 to the interface between domains B and C.

We then analyzed whether ME2 also has the AS1134900-binding site, given that AS1134900 did not detectably inhibit the enzymatic activity of ME2 (Figure 1D). Superposition of the crystal structure of the NADPH−AS1134900−ME1 complex with that of the open form of ME2[13] (PDB entry 1QR6) implies a potential pocket at the interface between domains B and C in ME2 (Figure 4B), though the cavity corresponding to the AS1134900-binding site of ME2 looks narrower than that of ME1 in molecular surface depiction (Figure 4A). On the contrary, the three-dimensional depiction of key amino acids for AS1134900 binding to ME1 and the corresponding residues of ME2 revealed that His 321 and Asp 360 in ME1 were Asn 321 and Tyr 361 in ME2, respectively (Figure 4C). While the imidazole moiety of His 321 is putatively required to interact with the imidazo[4,5-*b*]pyridine moiety of AS1134900 through $\pi-\pi$ stacking, Asn 321 is present in the corresponding position of ME2 and likely does not contribute to the binding. Similarly, ME2 Tyr 361 is positioned within the α-helix of domain B and sterically hinders the corresponding AS1134900-binding site of ME2. In addition, the benzene ring of ME2 Phe 263 is structurally flipped, preventing the formation of $\pi-\pi$ stacking with the

https://doi.org/10.1021/acs.biochem.2c00123
Biochemistry 2022, 61, 1548−1553

benzothiazole moiety of AS1134900. We presume that the differences among key amino residues likely explain the lack of affinity of AS1134900 for ME2. Future mutagenesis studies to evaluate the inhibitory activity of AS1134900 on N321H/Y361D ME2 or the resistance to AS1134900 inhibition on H320N/D361Y ME1 will be required to clarify the hypothesis.

Lastly, a parallel artificial membrane permeability assay (PAMPA) of AS1134900 was conducted to estimate the passive cell permeability of the small molecule. While Metoprolol, a high-permeability reference compound, demonstrated transfer into the acceptor side, AS1134900 had limited membrane passivity (Figure S5A). In addition, we tested the effects of AS1134900 on the viability of pancreatic cancer cell line PATU-8988T, in which knockdown of ME1 inhibits its clonogenic growth.[3] Consistent with the previous result,[3] glutamine was critical for the proliferation of PATU-8988T cells. On the contrary, AS1134900 did not reduce cellular proliferation (Figure S5B), perhaps owing to limited cell permeability.

Future directions will include structure−activity relationship analysis to increase the polar surface area of AS1134900, which will ultimately be necessary to evaluate the effects of this scaffold on ME1 in cancer cells. To this end, our report of the AS1134900-binding site on ME1 by X-ray crystal structure analysis of the ME1−AS1134900 complex may aid in the improvement of the chemical properties required for cell permeability. In summary, we describe the identification of a selective inhibitor of ME1, and its analysis in biochemical assays revealed a novel allosteric binding site. Future optimization of this lead scaffold is anticipated to provide a starting point for further discovery of drugs that inhibit ME1 activity in cancer cells.

■ ASSOCIATED CONTENT

Supporting Information

The Supporting Information is available free of charge at https://pubs.acs.org/doi/10.1021/acs.biochem.2c00123.

Detailed materials and methods and additional figures (PDF)

Accession Codes

Malic enzyme 1 (ME1), P48163; malic enzyme 2 (ME2), P23368.

■ AUTHOR INFORMATION

Corresponding Author

Costas A. Lyssiotis − *Department of Molecular & Integrative Physiology, Department of Internal Medicine, Division of Gastroenterology, and Rogel Cancer Center, University of Michigan, Ann Arbor, Michigan 48109, United States;* orcid.org/0000-0001-9309-6141; Email: clyssiot@med.umich.edu

Authors

Tomohiro Yoshida − *Business Development, Astellas Pharma Inc., Tsukuba, Ibaraki 305-8585, Japan*

Tetsuhiro Kawabe − *Applied Research & Operations, Astellas Pharma Inc., Tsukuba, Ibaraki 305-8585, Japan*

Lewis C. Cantley − *Meyer Cancer Center, Department of Medicine, Weill Cornell Medical College, New York, New York 10065, United States*

Complete contact information is available at: https://pubs.acs.org/10.1021/acs.biochem.2c00123

Funding

Research in the laboratory of L.C.C. was supported by National Cancer Institute Grant R35 CA197588.

Notes

The authors declare the following competing financial interest(s): T.Y. and T.K. are employees of Astellas Pharma Inc., and the research reported herein was funded by Astellas Pharma Inc. L.C.C. and C.A.L. received financial support from Astellas Pharma Inc. to conduct these studies. L.C.C. and C.A.L. are inventors on patents pertaining to Kras-regulated metabolic pathways, redox control pathways in pancreatic cancer, and targeting GOT1 or ME1 as a therapeutic approach. L.C.C. owns equity in, receives compensation from, and serves on the Scientific Advisory Boards of Agios Pharmaceuticals, Volastra Therapeutics, and Larkspur Biosciences. The laboratory of L.C.C. has previously received financial support from Petra Pharmaceuticals. Agios Pharmaceuticals is identifying metabolic pathways of cancer cells and developing drugs to inhibit such enzymes to disrupt tumor cell growth and survival. C.A.L. has received consulting fees from Astellas Pharmaceuticals, Odyssey Therapeutics, and T-Knife Therapeutics.

■ ACKNOWLEDGMENTS

The authors thank the high-throughput screening team and the pharmacokinetics team at Astellas Research Technology for their compound library screening efforts and PAMPA, Keiichiro Okuyama for a review of the method for the synthesis of AS1134900, Yusuke Tomimoto for ME1 protein purification, and Yasushi Amano for crystallographic experiments and refinement of structures.

■ REFERENCES

(1) Berg, J. M.; Tymoczko, J. L.; Stryer, L. *Biochemistry*, 5th ed.; 2002.

(2) Simmen, F. A.; Alhallak, I.; Simmen, R. C. M. Malic enzyme 1 (ME1) in the biology of cancer: it is not just intermediary metabolism. *J. Mol. Endocrinol.* **2020**, *65*, R77−R90.

(3) Son, J.; Lyssiotis, C. A.; Ying, H.; Wang, X.; Hua, S.; Ligorio, M.; Perera, R. M.; Ferrone, C. R.; Mullarky, E.; Shyh-Chang, N.; Kang, Y.; Fleming, J. B.; Bardeesy, N.; Asara, J. M.; Haigis, M. C.; DePinho, R. A.; Cantley, L. C.; Kimmelman, A. C. Glutamine supports pancreatic cancer growth through a KRAS-regulated metabolic pathway. *Nature* **2013**, *496*, 101−105.

(4) Hsieh, J. Y.; Li, S. Y.; Tsai, W. C.; Liu, J. H.; Lin, C. L.; Liu, G. Y.; Hung, H. C. A small-molecule inhibitor suppresses the tumor-associated mitochondrial NAD(P)+-dependent malic enzyme (ME2) and induces cellular senescence. *Oncotarget.* **2015**, *6*, 20084−20098.

(5) Wen, Y.; Xu, L.; Chen, F. L.; Gao, J.; Li, J. Y.; Hu, L. H.; Li, J. Discovery of a novel inhibitor of NAD(P) (+)-dependent malic enzyme (ME2) by high-throughput screening. *Acta Pharmacol. Sin.* **2014**, *35*, 674−684.

(6) Fernandes, M. X.; Padrón, J. M. Inhibition of Glutamine Metabolism as a Therapeutic Approach Against Pancreatic Ductal Adenocarcinoma. *Journal of Molecular and Clinical Medicine* **2019**, *2*, 97−110.

(7) Zhang, Y. J.; Wang, Z.; Sprous, D.; Nabioullin, R. In silico design and synthesis of piperazine-1-pyrrolidine-2,5-dione scafoldbased novel malic enzyme inhibitors. *Bioorg. Med. Chem. Lett.* **2006**, *16*, 525−528.

(8) Davis, M. I.; Shen, M.; Simeonov, A.; Hall, M. D. Diaphorase Coupling Protocols for Red-Shifting Dehydrogenase Assays. *Assay Drug Dev. Technol.* **2016**, *14*, 207−212.

(9) Yang, Z.; Lanks, C. W.; Tong, L. Molecular mechanism for the regulation of human mitochondrial NAD(P)+-dependent malic enzyme by ATP and fumarate. *Structure* **2002**, *10*, 951−960.

(10) Hsieh, J. Y.; Li, S. Y.; Chen, M. C.; Yang, P. C.; Chen, H. Y.; Chan, N. L.; Liu, J. H.; Hung, H. C. Structural characteristics of the nonallosteric human cytosolic malic enzyme. *Biochim. Biophys. Acta* **2014**, *1844*, 1773−1783.
(11) Yang, Z.; Zhang, H.; Hung, H. C.; Kuo, C. C.; Tsai, L. C.; Yuan, H. S.; Chou, W. Y.; Chang, G. G.; Tong, L. Structural studies of the pigeon cytosolic NADP+-dependent malic enzyme. *Protein Sci.* **2002**, *11*, 332−341.
(12) Yang, Z.; Floyd, D. L.; Loeber, G.; Tong, L. Structure of a closed form of human malic enzyme and implications for catalytic mechanism. *Nat. Struct. Biol.* **2000**, *7*, 251−257.
(13) Xu, Y.; Bhargava, G.; Wu, H.; Loeber, G.; Tong, L. Crystal structure of human mitochondrial NAD(P)(+)-dependent malic enzyme: a new class of oxidative decarboxylases. *Structure* **1999**, *7*, 877−899.
(14) Tao, X.; Yang, Z.; Tong, L. Crystal structures of substrate complexes of malic enzyme and insights into the catalytic mechanism. *Structure* **2003**, *11*, 1141−1150.
(15) Chang, G. G.; Tong, L. Structure and function of malic enzymes, a new class of oxidative decarboxylases. *Biochemistry* **2003**, *42*, 12721−12733.

https://doi.org/10.1021/acs.biochem.2c00123
Biochemistry 2022, 61, 1548−1553